

Characterizing Microstructural and Mechanical Properties of Al–Zn Alloys Processed by High-Pressure Torsion

Nguyen Q. Chinh,* Péter Szommer, Jenő Gubicza, Moustafa El-Tahawy, Elena V. Bobruk, Maxim Yu. Murashkin, and Ruslan Z. Valiev

Dedicated to Professor Terence G. Langdon on the occasion of his 80th birthday

Herein, the characterization of microstructures and mechanical properties of Al–Zn alloys ultrafine-grained (UFG) by using high pressure torsion (HPT) is surveyed. Emphasis is placed on the decomposition of the solid solution structures due to the HPT process, leading to unique mechanical and plastic properties of the UFG alloys. The decomposed microstructures, the grain boundaries wetted by Zn-rich layers, as well as the softening, grain boundary sliding (GBS) with usually high strain rate sensitivity and super-ductility of the HPT-processed samples are described and discussed. Furthermore, the innovation potential of intensive GBS at room temperature is briefly considered.

also on the grain-size, for instance, via the Hall–Petch equation^[21,22] describing the strengthening effect of the grain size, d , by

$$\sigma_y = \sigma_0 + A \cdot d^{-1/2} \quad (1)$$

where σ_y is the yield strength necessary for the onset of plasticity of a polycrystalline material, σ_0 is the friction stress, and A is a positive material constant related to the stress required to extend the dislocation activity into adjacent grains. Equation (1) demonstrates that for a given composition, the yield strength increases with decreasing

the grain size. Furthermore, taking into account also the important role of grain size in superplastic deformation by considering the constitutive equation^[23–26]

$$\dot{\varepsilon} = A^* \frac{D \cdot \mu \cdot b}{k \cdot T} \left(\frac{b}{d} \right)^p \left(\frac{\sigma}{\mu} \right)^q \quad (2)$$

where $\dot{\varepsilon}$ is the strain rate of the superplastic flow, D is the coefficient of grain-boundary diffusion, μ is the shear modulus of the investigated material, b is the magnitude of the Burgers vector, k is the Boltzmann constant, T is the absolute testing temperature, p is the grain-size exponent, σ is the flow stress of the deformation process, q is the stress exponent, and A^* is a dimensionless constant, it can be expected that a decrease of grain-size, d , should improve the occurrence of superplasticity at relatively low temperatures and/or relatively high strain rates.

The improvements in the strength and ductility of materials would have positive economic impacts. The significance of both Equation (1) and (2) was a strong motivation of several first efforts to get finer grain sizes in conventional materials using severe plastic deformation (SPD).^[26–32] In the last two decades, the application of SPD processing has shown the possibility to change the grain size significantly and the mechanical properties of many metals and alloys. Several methods such as high-pressure torsion (HPT),^[26,27,32–39] equal-channel angular pressing (ECAP),^[31,40–47] and accumulative roll-bonding (ARB)^[48,49] were used to apply SPD on different materials.

In this review, some recent results on the characterization of microstructural and mechanical properties of HPT-processed Al–Zn alloys are summarized. The main results contain the grain refinement and decomposition of the microstructures, the formation of special grain-boundaries leading to intensive grain

1. Introduction

It is well-known that among the binary Al-based alloys, the best known Al–Zn system is particularly suitable for studying the mechanisms and kinetics of both solid solution- and precipitation-strengthening.^[1] Some typical compositions, such as eutectic Al–95 wt% Zn, eutectoid Al–70 wt% Zn, and solid solutions with Zn contents lower than 31.6 wt%, have been extensively studied.^[2–20]

In general, the mechanical and plastic behavior of a given material is dominantly determined by its microstructure, which depends not only on the chemical and phase compositions but

Prof. N. Q. Chinh, P. Szommer, Prof. J. Gubicza
Department of Materials Physics
Eötvös Loránd University
Pázmány Péter sétány 1/A., Budapest H-1117, Hungary
E-mail: chnh@metal.elte.hu

Dr. M. El-Tahawy
Department of Physics
Faculty of Science
Tanta University
31527 Tanta, Egypt

Dr. E. V. Bobruk, Dr. M. Y. Murashkin, Prof. R. Z. Valiev
Institute of Physics of Advanced Materials
Ufa State Aviation Technical University
12 K. Marx street, Ufa 450008, Russia

Prof. R. Z. Valiev
Laboratory of Mechanics of Advanced Bulk Nanomaterials
Saint Petersburg State University
Universitetskii prospekt 28, Peterhof, St. Petersburg 198504, Russia

 The ORCID identification number(s) for the author(s) of this article can be found under <https://doi.org/10.1002/adem.201900672>.

DOI: 10.1002/adem.201900672

boundary sliding (GBS), as well as the unique plastic behaviors of these materials. Possible practical importance of intensive GBS is also reviewed.

This article summarizes several results of previous joint researches where the present authors have had opportunities to cooperate with Professor Terence G. Langdon. We have learnt so much from Langdon about the superplasticity of ultrafine-grained (UFG) materials, the important role of GBS, and so on. We could count on his assistance almost at any time, remotely by e-mail or personally in conferences, workshops. Hereby, the authors would like to express their warm thanks to Prof. Terence G. Langdon and are glad to contribute to this special issue honoring his anniversary.

2. Characterization of the Microstructure of HPT-Processed Al–Zn Alloys

2.1. Grain-Refinement and Decomposition

Al–Zn alloys having a Zn content from 2 to 30 wt% were obtained from high purity (5N Al and also 5N Zn) components. After casting, the billets were homogenized at 500 °C for 5 h. The homogenized microstructures have a grain size of about 60–70 μm. Disc-shaped samples having a diameter of 20 mm and a thickness of 1.4 mm were fabricated and always (again) homogenized at 500 °C for 1 h, followed by room temperature (RT) water quenching to get solid solution state immediately before HPT processing. The homogenized discs were processed by HPT^[8,13,14] at a rotation speed of 1 rpm, applying a pressure of 6 GPa. All studies in this subject have shown a significant grain-refinement and a decomposition of the microstructure in the Al–Zn samples after HPT-processing up to 10 revolutions at RT). The final grain size was lower than 1 μm and depended on the Zn content. The average grain-size of Al–2 wt% Zn, Al–5 wt% Zn, Al–10 wt% Zn, and Al–30 wt% Zn alloys were about 950, 500, 435, and 350 nm, respectively.^[14] Hereafter, these compositions are denoted as Al–2Zn, Al–5Zn, Al–10Zn, and Al–30Zn, respectively. The transmission electron microscopy (TEM) images in **Figure 1** show, for instance, the microstructure of the HPT-processed Al–30Zn sample.

In addition to the grain refinement, HPT processing has also resulted in decomposition of the solid solution states, as shown in **Figure 1b** for Al–30Zn sample. The experimental results^[8] showed that Zn particles formed in the triple junctions of Al/Al grain boundaries and also inside the Al grain interiors. The size and distribution of the Zn particles formed during HPT processing depend on the Zn content. In the case of the lowest Zn-concentrated Al–2Zn alloy, Zn particles with the size lower than 20 nm can be found,^[14] but for the high Zn contents of 10 and 30 wt%, well-developed particles of about 150–200 nm are formed in the triple junctions of the Al grains. For these higher Zn-containing alloys, smaller Zn particles with the size of only 5–15 nm can also be observed inside the Al grains (**Figure 1b**).

Concerning the characteristics of the HPT-processed samples, **Figure 2** shows the dislocation density and the coherent domain size of the Al matrix as a function of the nominal Zn concentration.^[18] It can be seen that both parameters are “normally” changing, similar to the behavior of Al–Mg alloys.^[50] Due to



Nguyen Quang Chinh graduated in Physics from Eötvös Loránd University in 1985. Since then he has been working in various fields of materials science. His recent main research topics are 1) plastic behavior and strengthening mechanisms of metals and alloys, 2) microstructural and mechanical characteristics of ultrafine-grained and nanocrystalline materials, and 3) development of the depth sensing indentation method, taking in several international cooperation. Currently he is the leader of the Hungarian group in a joint project with Russian researchers entitled “Study of the phenomenon of grain boundaries and development of low-temperature superplastic forming of high-strength ultrafine-grained aluminum alloys.”



Ruslan Z. Valiev (Ufa, Russia) established the vision for the potential of bulk nanostructured materials and pioneered the development of severe plastic deformation (SPD) as the effective process by which these materials can be produced and used in engineering and medicine. He is among the most highly cited scientists in the world in the area of nanomaterial science and his main present research interests comprise studies of superior mechanical and functional properties of SPD produced nanomaterials.

the pinning effect of the solute atoms and precipitates, the dislocation density increases and correspondingly the coherent domain size decreases with increase in Zn concentration. It should be noted that the coherent domain size corresponds to the subgrain size; therefore, it is smaller than the grain size determined by microscopy.

2.2. Grain Boundaries Wetted by Zn-Rich Layers in HPT-Processed Al–Zn Alloys

Together with the grain refinement and the decomposition of the solid solution into Al matrix and Zn particles, microstructural investigations taken by using TEM and energy-dispersive X-ray spectroscopy (EDS)^[12,14,20] have also revealed a special structure of the grain boundaries wetted by the segregation of Zn solute atoms in high Zn-containing Al–10Zn and Al–30Zn alloys. In the case of Al–30Zn sample, more than 50% of the Al/Al grain boundaries is wetted by Zn-rich layers as shown in Z-contrast high-angle annular dark field (HAADF) image and EDS mapping of **Figure 3**.

A wetting layer having thickness of about 2 nm can be seen in the high-resolution transmission electron microscopy (HRTEM) image of **Figure 4**. It should be noted that the phenomenon of deformation-induced phase transformation as the decomposition of a supersaturated solid solution is well-established in other alloys, for instance, in Al–Mg^[3] and Cu-based alloys.^[51]

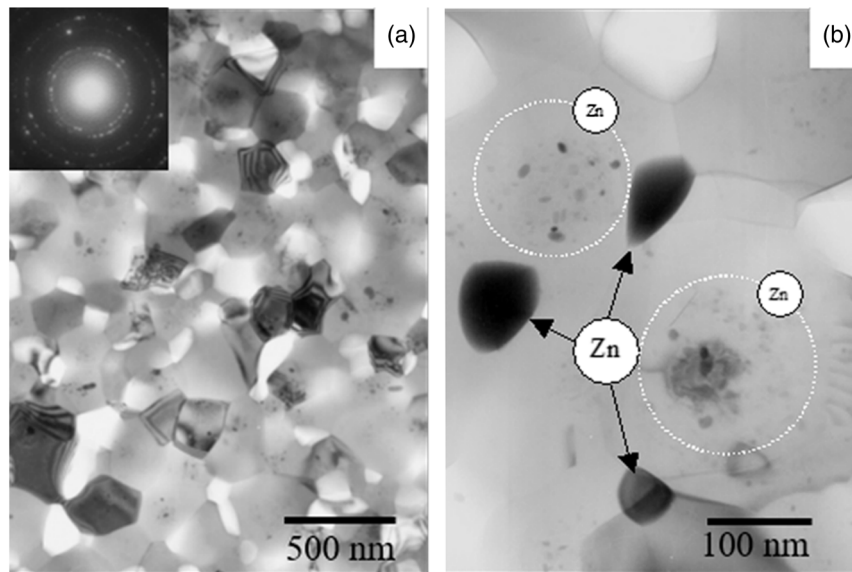


Figure 1. Microstructure of the HPT-processed Al–30Zn sample, showing a) the UFG microstructure and b) Zn particles at triple junctions of Al/Al boundaries and within Al grains. Reproduced with permission.^[8] Copyright 2010, Springer.

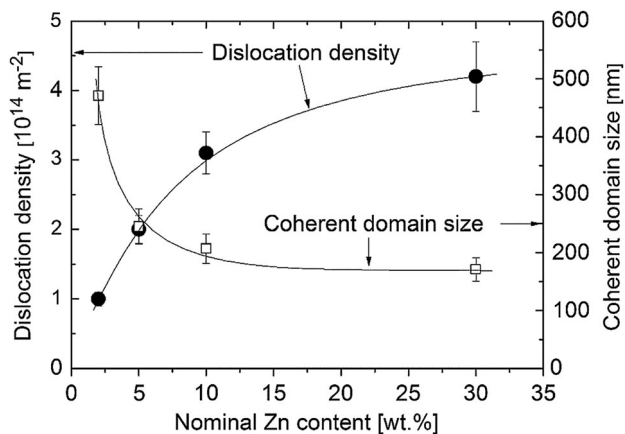


Figure 2. Effect of HPT processing on the dislocation density and coherent domain size as a function of the nominal Zn concentration. Reproduced with permission.^[18] Copyright 2017, Elsevier.

In the present case of Al–Zn alloys, the Al grains, Zn particles, and the Zn-rich layers formed due to the decomposition are certainly new components in the decomposed microstructure. It can be expected that the decomposed microstructure will change significantly the mechanical and physical behaviors of the original alloys. Before reviewing the mechanical and plastic properties of the HPT-processed Al–Zn samples, let us see the effect of the decomposed microstructures on the thermal stability studied by calorimetry.

2.3. The Effect of the Decomposition on the Differential Scanning Calorimetry Thermograms

Typical differential scanning calorimetry (DSC) thermograms^[18] taken on the HPT-processed Al–Zn samples with different Zn

contents can be seen in **Figure 5a**. The curves obtained for the HPT-processed Al–30Zn sample is plotted together with that of the annealed state in **Figure 5b**. It can be seen that the thermogram of the annealed sample has well-defined endothermic peaks indicating the dissolution of Guinier–Preston (GP) zones and the solution of Zn in Al.^[52] However, for the HPT-processed Al–30Zn sample, the first DSC peak was not observed, as SPD facilitated the development of Zn particles without the formation of metastable GP zones.

Comparing the thermograms of the HPT samples with different (2, 5, 10, and 30 wt%) Zn contents (**Figure 5a**), it can be seen that there is a conspicuous difference between the Al–30Zn sample and the other three lower Zn-concentrated alloys. A double-peak thermogram is observed only for Al–30Zn sample, which consists of two peaks located at $T = 525$ and 555 K. The first peak at 525 K, which is similar to the second peak of the annealed state, corresponds to the dissolution of Zn in Al (see **Figure 5b**). The second endothermic peak at 555 K for the HPT-processed Al–30Zn sample most probably indicates the dissolution of the Zn-rich boundary layers. This second peak cannot be observed at lower Zn contents. Therefore, the presence of this peak indicates the significant amount of the Zn-rich layers in the Al–30Zn alloy.

In the light of decomposed UFG microstructure, let us review now the mechanical and plastic behaviors of the investigated Al–Zn samples.

3. Characterization of the Mechanical Properties of the HPT-Processed Al–Zn Alloys

3.1. The Normal Strengthening and Abnormal softening

Figure 6 shows the effect of Zn concentration on the hardness of the HPT-processed Al–Zn alloys. For comparison, the hardness values of the annealed samples are also plotted in **Figure 6**.

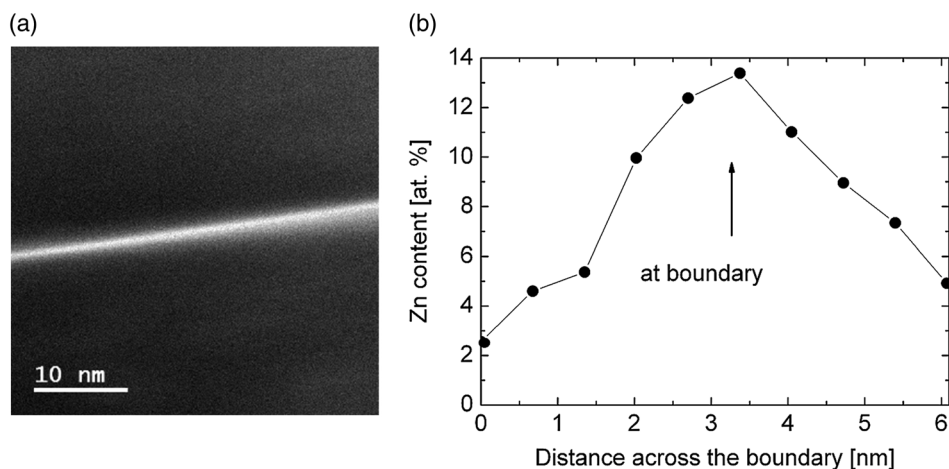


Figure 3. Zn-rich layer at an Al/Al grain boundary in the HPT-processed Al-30Zn alloy, demonstrated by a) TEM and b) results of EDS line profile analysis. Reproduced with permission.^[12] Copyright 2014, Wiley.

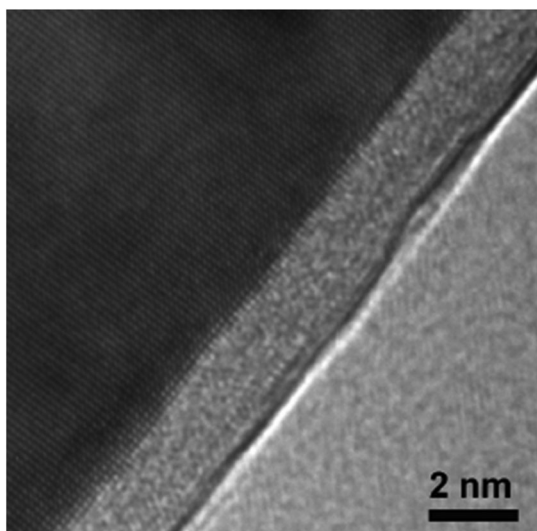


Figure 4. HRTEM image showing a wetting layer along an Al/Al grain boundary in the HPT-processed Al-30Zn sample. Reproduced with permission.^[20] Copyright 2014, Elsevier.

For Zn concentrations not more than 10 wt%, the normal strengthening effect of SPD can be observed as the hardness of the HPT-processed samples is higher than that of the annealed samples. In the case of the Al-30Zn alloy, however, there is a strong reduction in hardness, indicating an abnormal softening due to HPT. The abnormal softening of the high Zn-concentrated Al-30Zn alloy is certainly a consequence of the mentioned strong decomposition of the annealed microstructure in this alloy,^[12] leading to significant decrease of the strengthening effect of the (Zn) solute atoms.

The abnormal softening of the HPT-processed UFG Al-30Zn sample was studied also by nanoindentation.^[12] To emphasize the significant changes, the indentation behavior of the HPT-processed Al-30Zn sample is compared with that of the coarse-grained (annealed) counterpart having the same composition,

as well as with that of coarse-grained and UFG pure Al.^[12] A series of 400 nanoindentation measurements were made at a low maximum load of 0.5 mN so that the size of the indentation pattern was close to or smaller than the grain size in this UFG sample. Under these conditions, the indentation measurements were carried out mainly on individual grains in both the UFG Al and Al-30Zn samples. **Figure 7** shows some typical load–depth ($F-h$) indentation curves (Figure 7a) and the distribution of the nanohardness (Figure 7b) obtained for the investigated samples. It can be seen that the behavior of the UFG Al-30Zn sample is rather similar to that of the UFG pure Al, and although the UFG Al-30Zn is harder than the coarse-grained Al, it is much softer than the coarse-grained annealed Al-30Zn sample, also indicating the mentioned abnormal softening due to HPT processing.

3.2. Characteristics of Plastic Deformation

Several investigations of the plastic behaviors of materials are rather focused on strain rate sensitivity (SRS) because it is well established that this parameter correlates to the ductility.^[53] Because of the significance of this parameter, several methods were developed for determinations of the SRS, including the conventional tensile testing,^[54–59] impression creep^[60–62] and depth-sensing indentation testing^[63–67] techniques.

Recent experimental results have also shown a correlation between SRS and viscous properties of UFG Al-Zn alloys.^[68] The SRS values determined by applying the indentation creep method^[65] on the HPT-processed Al-Zn samples are 0.08, 0.14, 0.17, and 0.25 for Al-2Zn, Al-5Zn, Al-10Zn and Al-30Zn, respectively.^[18] Experimental results show that the SRS increases with Zn content, and an unusually high value (0.25) was obtained for the Al-30Zn alloy. In general, the UFG materials produced by SPD exhibit extremely low SRS of about 0.01–0.03.^[69] In the present case, the relatively high SRS should be attributed to the Zn addition. Furthermore, the unexpectedly high SRS obtained for the HPT-processed Al-30Zn sample is a consequence of the high fraction of Al/Al grain boundaries wetted by Zn-rich layers,

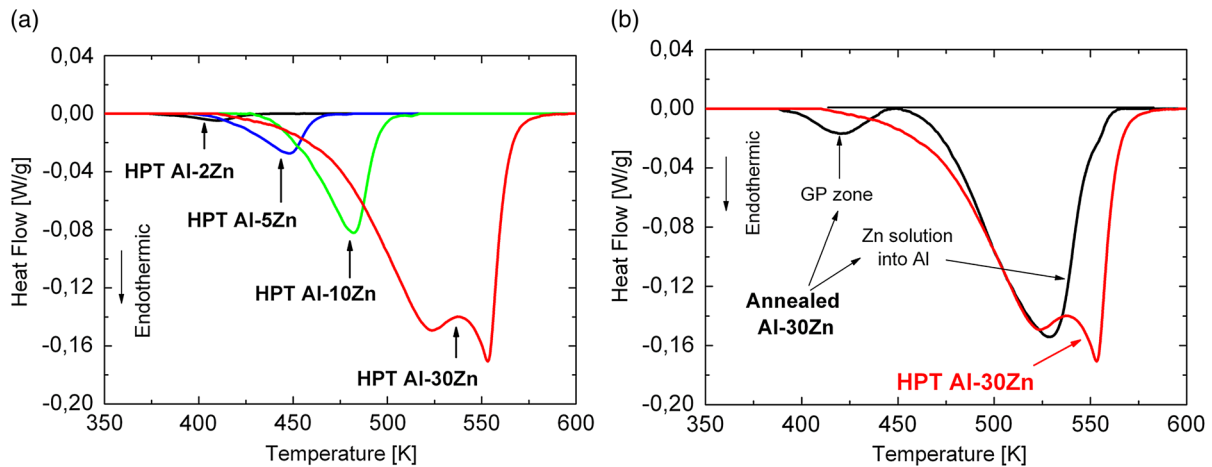


Figure 5. DSC thermograms taken at a heating rate of 20 K min^{-1} on a) HPT-processed Al–Zn alloys with different Zn contents and b) both annealed and HPT-processed Al–30Zn samples. Reproduced with permission.^[18] Copyright 2017, Elsevier.

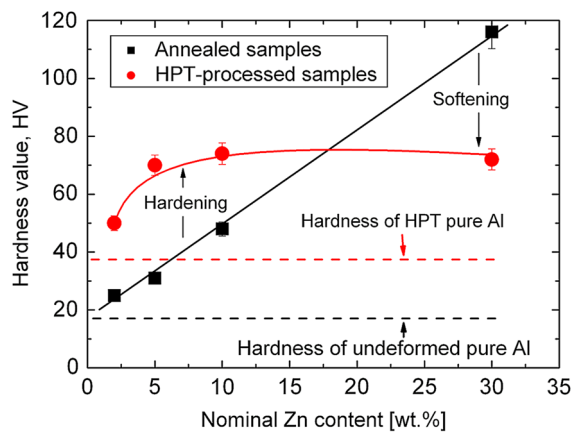


Figure 6. Effect of HPT processing on microhardness of different Al–Zn alloys, showing both “normal” strengthening and “abnormal” softening. Reproduced with permission.^[18] Copyright 2017, Elsevier.

which lead to intensive GBS and then to a super-ductility,^[8] as shown in **Figure 8**.

The stress–elongation curves of **Figure 8** demonstrate that both the stress and the total elongation of the Al–30Zn samples deformed at RT depend strongly on the strain rate. The HPT-processed UFG Al–30Zn samples exhibit unusually high ductility of about 160% when testing at strain rate of 10^{-4} s^{-1} at RT.^[8]

To characterize the role of the grain boundaries, nanoindentation measurements were made in different conditions, causing plastic deformation at different scales.^[11] A series of 400 nano-indentation measurements were made first at a very low maximum load of 0.5 mN—similar to the conditions of measurements presented in **Figure 7**—so that the size of the indentation pattern was about equal to the average grain size of the UFG Al–30Zn alloy. In this case, as it has already been mentioned, most probably the measurements were carried out on individual grains in both UFG Al and Al–30Zn samples. **Figure 9** shows the distribution of

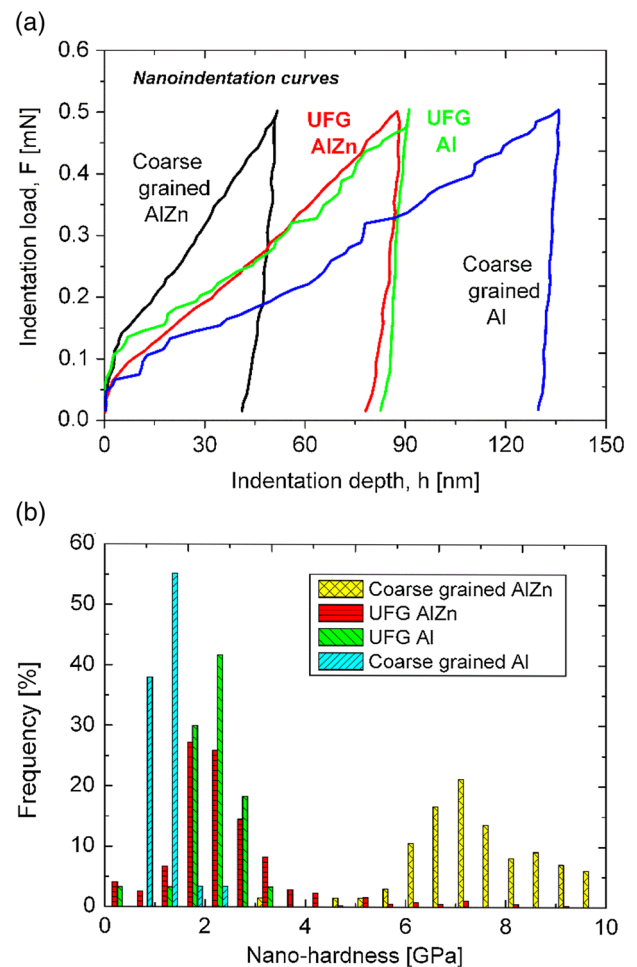


Figure 7. a) Typical indentation depth–load curves obtained on different materials and b) distribution of the nano-hardness, demonstrating the abnormal softening of the HPT-processed UFG Al–30Zn alloy. Reproduced with permission.^[12] Copyright 2014, Wiley.

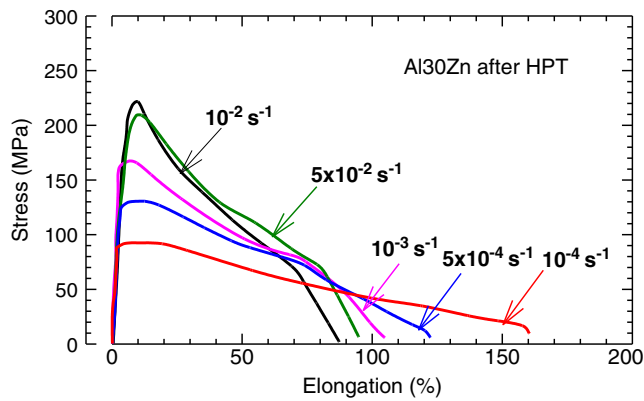


Figure 8. Stress–strain curves obtained at different strain rates on HPT-processed Al–30Zn samples deformed by tensile test, showing the super-ductility of this sample at RT. Reproduced with permission.^[8] Copyright 2010, Springer.

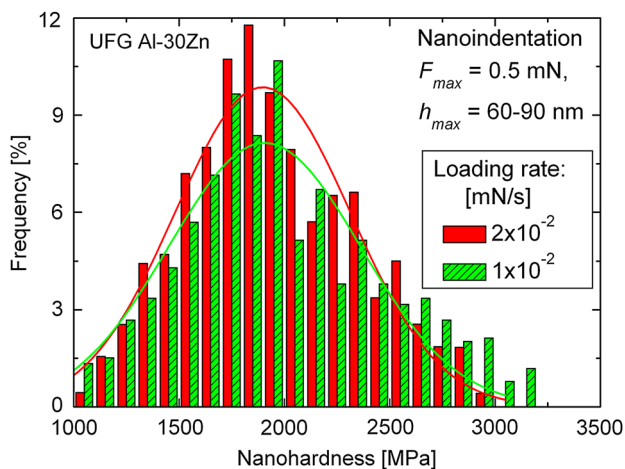


Figure 9. The distribution of hardness obtained at the maximum load of 0.5 mN with two different loading rates on UFG Al–30Zn alloy. The solid lines indicate Gaussian fit of the spectra, showing the very low sensitivity of the deformation process in small (about one grain) scale. Reproduced with permission.^[11] Copyright 2012, Elsevier.

the nanohardness obtained for different loading rates on the UFG Al–30Zn sample. It can be seen that these nanohardness spectra are almost the same, indicating that under this condition, the nanohardness of UFG Al–30Zn is not sensitive to the loading rate. This means that when only one grain is deformed in UFG Al–30Zn, the SRS is very low so that the deformation process or the nanohardness is not sensitive to the strain rate.^[11]

When the maximum load was increased to 1 mN, the size of the indentation pattern was $\approx 1\text{--}1.5\ \mu\text{m}$, which is about 3–4 times larger than the average grain size of the UFG Al–30Zn alloy so that the indentation pattern covers a group of at least $\approx 5\text{--}7$ grains. In this case, the experimental results shown in **Figure 10a** reveal that the distribution of the nanohardness obtained on the UFG Al–30Zn alloy becomes sensitive to the loading rate. Fitting Gaussian functions to the measured spectra and taking the peak value, similar to the results of the mentioned indentation creep

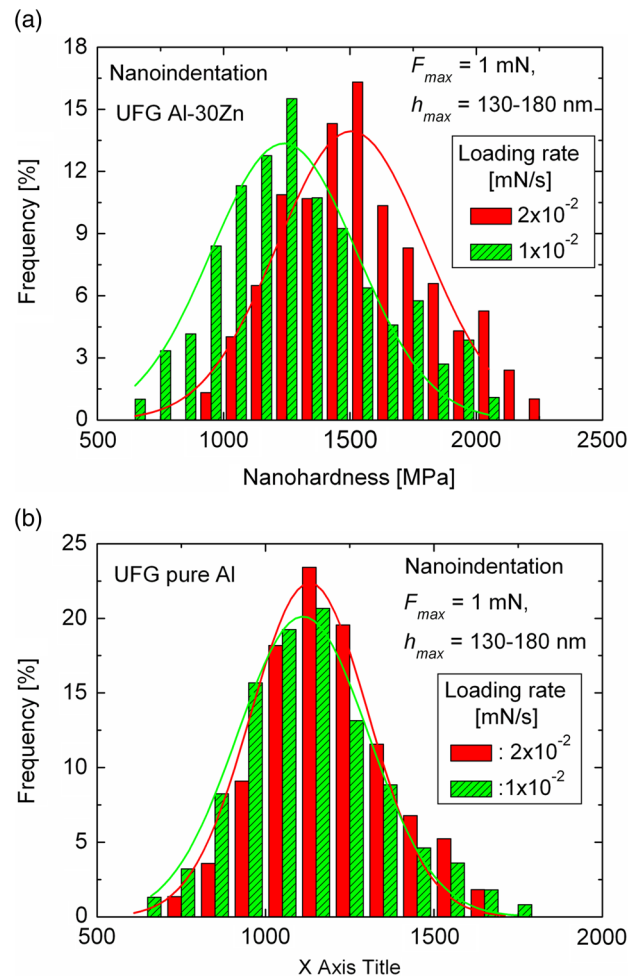


Figure 10. The distribution of nanohardness obtained at the maximum load of 1 mN with two different loading rates on a) UFG Al–30Zn alloy and b) UFG pure Al. The solid lines indicate the Gaussian fit of the spectra, showing the higher sensitivity of the deformation process in larger (a group of several grains) scale in the case of UFG Al–30Zn sample. Reproduced with permission.^[11] Copyright 2012, Elsevier.

method,^[18] a SRS of $m \approx 0.25$ was estimated. This result shows clearly that, when a group of grains is plastically deformed in the UFG Al–30Zn alloy, the role of the grain boundaries should be taken into account. The nanoindentation results presented in **Figure 10b** confirm the low SRS of UFG pure Al as the nanohardness distribution of this material appears insensitive to the loading rate.^[11]

Performing microhardness measurements at different testing temperatures, the activation energy characterizing the process of plastic deformation in the UFG Al–30Zn alloy has been determined.^[11] The experimentally determined activation energy of $65\ \text{kJ mole}^{-1}$ ^[11] is lower than the values for self-diffusion in Al ($142\ \text{kJ mole}^{-1}$ ^[70]), self-diffusion in Zn ($92\ \text{kJ mole}^{-1}$ ^[70]), or grain boundary diffusion in Al ($84\ \text{kJ mole}^{-1}$ ^[70]). Therefore, it can be supposed that in the UFG Al–30Zn the process of plastic deformation is controlled neither by the self-diffusion of Al nor by the self-diffusion of Zn atoms.

Using some reasonable parameters,^[11] the diffusion coefficient in the UFG Al–30Zn alloy was estimated as having a value that correlates with the measured, relatively high diffusivity ($\approx 10^{-15} \text{ m}^2 \text{ s}^{-1}$) for Zn along Al/Al grain boundaries.^[71,72] This suggests that the process of plastic deformation in UFG Al–30Zn alloy at RT is controlled mainly by Zn diffusion along the Al/Al grain boundaries, emphasizing the importance of the Zn-rich layers covering Al/Al boundaries in the UFG Al–Zn alloys. The accelerated diffusion of Zn along the Al/Al boundaries may serve to enhance the development of GBS. It has been reported earlier^[7] that the fraction of Al/Al boundaries plays a critical role in the Zn–22% Al eutectoid alloy processed by SPD, as these boundaries generally exhibit an essentially lower sliding contribution than the Zn–Zn and Zn–Al boundaries.

Both the high diffusivity and the mentioned high SRS are predicting significant role of GBS in the UFG Al–30Zn alloy, leading to the super-ductility and even superplasticity (over 400% tensile elongations) at RT, as it was recently shown on the UFG alloy Al–30 at%Zn (Al–60 wt%Zn)^[73] tested at strain rate of $5.5 \times 10^{-5} \text{ s}^{-1}$. To check experimentally this prediction, as well as the relationship between SRS and plasticity, micropillars (having diameters of $\approx 3 \mu\text{m}$ and heights of $\approx 10 \mu\text{m}$) were prepared and deformed by nanocompression.^[12] In the next section, some examples for micropillar compressions will be overviewed.

3.3. Intensive GBS at RT and its Effect on the Deformation Process

For the micropillars deformed by compression, it should be noted that the pillars fabricated on the surface of the UFG Al–30Zn sample having a grain size of $\approx 300\text{--}400 \text{ nm}$ can be regarded as polycrystalline specimens at the micro scale. The micropillars in the annealed, coarse-grained samples, however, are rather single crystals. **Figure 11** shows a scanning electron microscopy (SEM) image presenting the preparation process of the pillars on the coarse-grained Al–30Zn sample. Four pillars can be seen on three grains having different orientations (see Figure 11a). The orientations of these grains were determined using the electron back-scattered diffraction (EBSD), as shown in Figure 11b.

Figure 12 shows some stress–strain curves characterizing the compression of micropillars on the surfaces of both coarse-grained annealed and UFG Al–30Zn samples. It can be seen that the flow stresses of the coarse-grained Al–30Zn samples are much higher than that of the UFG alloy, again expressing the abnormal softening of the HPT-processed sample.

Considering the deformation of the micropillars, further significant differences can be observed between the behaviors of the coarse-grained and UFG materials. While the compression curves of the coarse-grained samples show the presence of visible strain avalanches, the curves obtained for the UFG pillars are smooth and there is a marked absence of any strain avalanches.^[12]

Strain avalanches are well-known phenomena characterizing the plasticity of micrometer-scale single crystals.^[74–79] In the case of the UFG polycrystalline micropillars, however, the role of the grain boundaries must be taken into consideration, when interpreting the plastic behavior of these UFG samples. In this context, grain boundaries can act as obstacles against moving

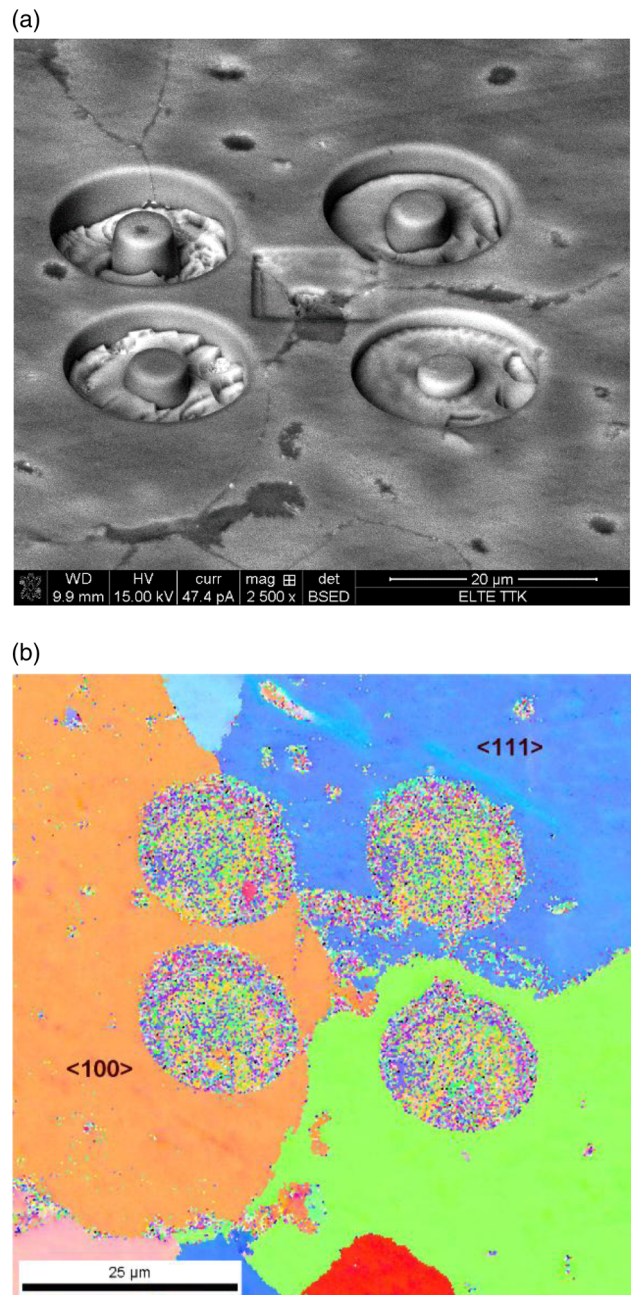


Figure 11. Images demonstrating the preparation of micropillars on the annealed, coarse-grained Al–30Zn sample, showing a) the beginning of the milling by focused ion beam (FIB) and b) the orientation of the pillars detected by EBSD. There is a triple junction of three grains having different crystallographic orientations in the middle of the image, showing the grains having orientation near $\langle 100 \rangle$ and $\langle 111 \rangle$ on left and upper right, respectively. Reproduced with permission.^[12] Copyright 2014, Wiley.

dislocations but also they may become sources for dislocations. Furthermore, if grain boundary diffusion is accelerated, leading to the occurrence of significant GBS, the deformation process will take place primarily through the motion of grain boundaries. Because of these compensating effects, it follows that strain avalanches cannot take place in the polycrystalline pillars and

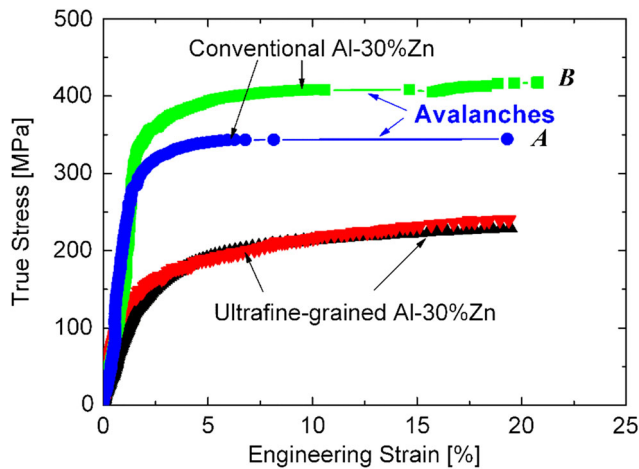


Figure 12. Typical compression stress–strain curves obtained for micropillars on the surface of both coarse-grained and HPT-processed UFG Al–30Zn samples, demonstrating strain avalanches in the single crystal pillars on the coarse-grained sample, and smoothly stable deformation without avalanches in the UFG pillars. The single crystal pillars A and B have orientations near $\langle 100 \rangle$ and $\langle 111 \rangle$, respectively. Reproduced with permission.^[12] Copyright 2014, Wiley.

therefore the smooth flow of the UFG samples should be attributed to the effect of the grain boundaries.

The examination of the compressed micropillars by SEM has also revealed significant differences between the surface morphologies of the coarse-grained and UFG samples. **Figure 13** shows typical surface morphologies of both samples. In the case of the coarse-grained sample (see Figure 13a,b) strain localizations and extreme slip bands are observed near to the direction of maximum shear stress at 45° relative to the orientation of the compression stress. By contrast, no strain localizations and extreme slip bands can be observed on the surface morphologies of the compressed UFG micropillars as shown in Figure 13c,d in different magnifications.

It is well-established that the mechanism of GBS can be made visible by using atomic force microscopy (AFM).^[8,80,81] **Figure 14** shows an indentation pattern formed by pressing a Vickers indenter on the surface of an UFG Al sample. Analyzing the morphology of the surface around the pattern, it can be seen that there is a rumpling around the indentation, which corresponds to the movement of grains within the UFG matrix. It can be concluded that the grains having a size of about $1 \mu\text{m}$ move with respect to each other, providing a good evidence for the occurrence of intensive GBS as a significant mechanism for deformation process of UFG pure Al at RT.^[81]

It is also well known that GBS is the main mechanism for high temperature superplastic deformation,^[82–84] which is generally

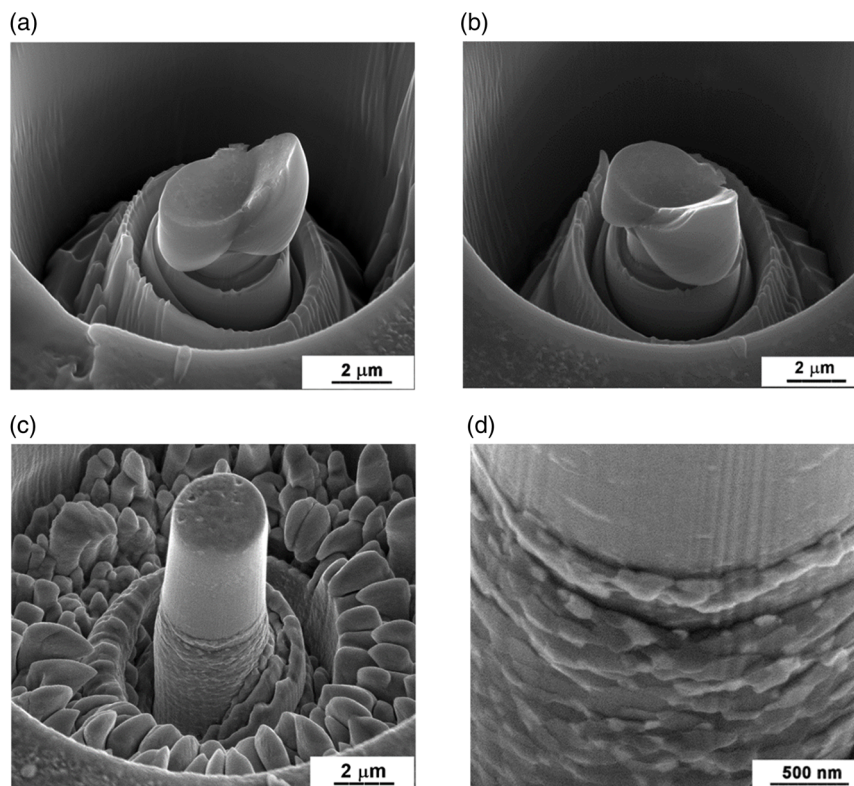


Figure 13. The surface morphologies of the deformed micropillars on the surface of a,b) the coarse-grained Al–30Zn sample in two different positions (separated by 60° rotation), demonstrating strain localizations and extreme slip bands corresponding to the avalanches visible on sample A in Figure 12. c,d) the HPT-processed UFG Al–30Zn sample at low and high magnifications, respectively, showing a direct evidence for the occurrence of intensive GBS without strain localizations and extreme slip. Reproduced with permission.^[12] Copyright 2014, Wiley.

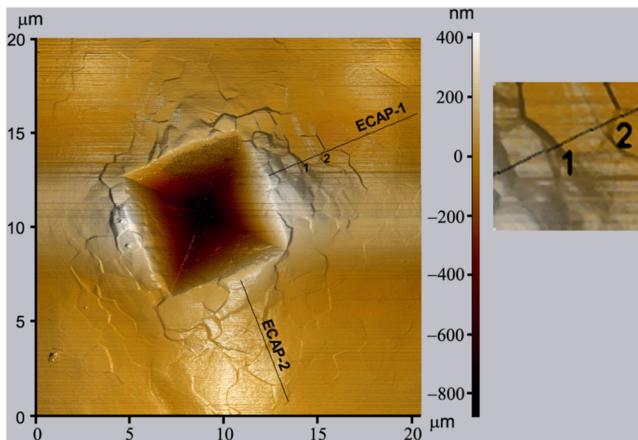


Figure 14. An AFM image of the surface of a UFG pure Al sample deformed by indentation using a Vickers indenter. Reproduced with permission.^[81] Copyright 2006, Elsevier.

characterized by a relatively high SRS. In the case of UFG pure Al, despite the significant role of GBS, the value of SRS and the ductility is very low. As it has been mentioned, in general, a low value between 0.01 and 0.03 is typical for the SRS of face-centered cubic (fcc) metals deformed at low temperatures.^[69] Comparing with the plastic properties of the UFG Al alloy, the behavior of the HPT-processed UFG Al–30Zn is quite unique and prominent due to its superductility with a total elongation higher than 150% and a corresponding unusually high SRS at RT.

The unique properties of the HPT-processed Al–30Zn alloy at RT are due to the special sliding of grain boundaries wetted by thin Zn layers. **Figure 15** shows a typical AFM image of the surface pattern after indentation with a Vickers indenter on the UFG Al–30Zn sample.^[8] It can be observed that the surrounding area of the Vickers pattern looks like it has been scattered by

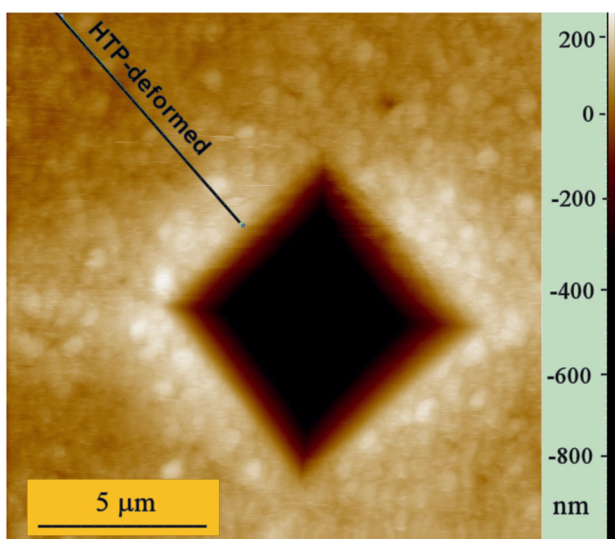


Figure 15. An AFM image of the surface of the UFG Al–30Zn sample deformed by indentation using a Vickers indenter. Reproduced with permission.^[8] Copyright 2010, Springer.

“sand-like” grains having a size of about 400 nm. Detailed measurements^[8] have revealed that, similar to the situation shown in Figure 14 for UFG pure Al, the rumpling picture also corresponds to the movements of the individual ultrafine grains within the ultrafine crystalline matrix.

Considering the relationship between SRS and the contribution of GBS to the total deformation process, it should be emphasized that while there is a significant difference between SRS of UFG Al and UFG Al–30Zn, there is no quantitative difference in the contribution of GBS for these two materials. This contribution to the total deformation process has been measured as 50%–60% for both materials,^[8,80,81] but the SRS of the UFG Al is very low, only about 0.03.^[11] An interpretation has been given by considering the shapes of the pile-ups around the Vickers patterns shown in Figure 14 and 15, where there is a significant qualitative difference in the flow process for these two materials.^[11,19]

Figure 16a shows typical vertical profiles across the Vickers indentation patterns for the UFG pure Al and UFG Al–30Zn

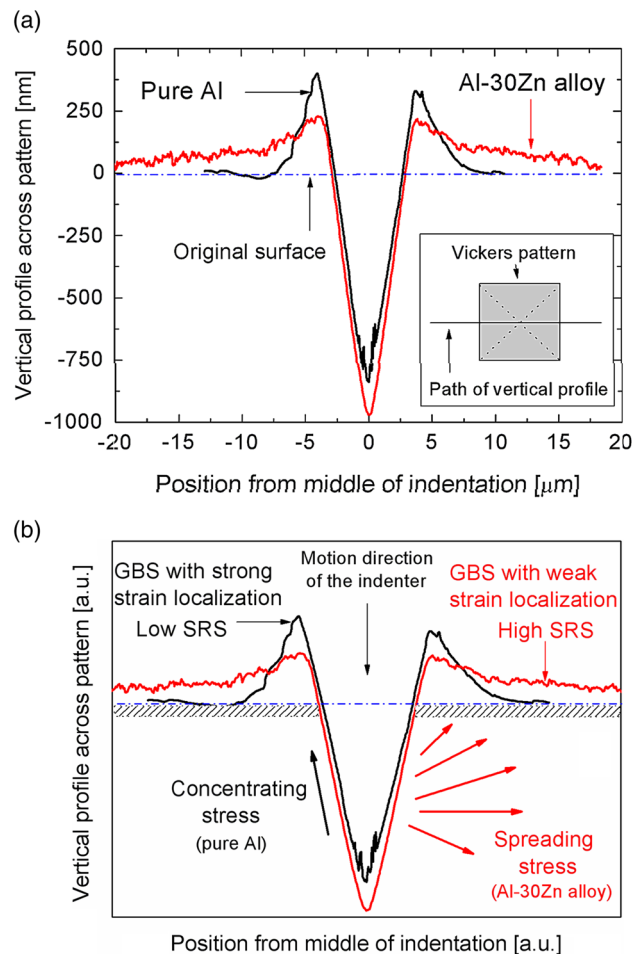


Figure 16. Vertical profiles across the centers of the Vickers patterns a) showing the development of pile-ups as qualitative difference in GBS of UFG pure Al and Al–30Zn and b) schematically demonstrating the deformation profile under the Vickers indenter and the correlation between GBS and SRS. Reproduced with permission.^[19] Copyright 2011, Trans Tech Publication.

presented in Figure 14 and 15, respectively. These profiles reveal that the pile-ups formed on the surface of UFG pure Al are short-range and appear sharp only in the close vicinity of the Vickers pattern whereas in the case of the UFG Al–30Zn alloy the pile-ups seem to be long-range and spread over relatively long distances from the Vickers pattern. This difference can be explained by the significantly higher mobility of the Zn-wetted grain boundaries in the Al–30Zn alloy, the behavior of which tends to that of liquids, so that this UFG material becomes super-ductile at RT. This difference in the flow process correlates directly with the values of the SRS of these two materials, as illustrated schematically in Figure 16b. In the case of UFG Al–30Zn alloy, because of a relatively high SRS, high pile-ups cannot form around the Vickers pattern, which is similar to the phenomenon in tensile testing when the strain/stress will not concentrate locally so that a neck is not formed. Instead, the pile-ups spread over a large area, homogenizing the deformation and consequently leading to the super-ductility of this alloy at RT. Physically, the higher SRS of the HPT-processed UFG Al–30Zn hinders more effectively the local deformation in the vicinity of the Vickers pattern where the strain and the strain rate are the highest. In this way, the deformation process tends to spread over larger distances from the pattern.

4. Innovation Potential of Intensive GBS at RT

Let us review the deformation processes occurring in the coarse-grained and UFG micropillars shown in Figure 12. The significant differences between the deformation of these samples can be interpreted using the results of the SEM investigations shown in Figure 13. The strain localizations and extreme slip bands observed in the coarse-grained samples (Figure 13a,b) correlate directly with the strain avalanches visible in the compression curves of the micropillars for the coarse-grained samples (Figure 12). In general, the large strain fluctuations may lead to uncertainties in plastically forming micrometer-scale single crystals because of the possibility of catastrophic failure.^[75] For this reason, in practical application, micrometer-sized samples of coarse-grained metals are not suitable for use in the fabrication of microdevices.

By contrast, no strain localizations or extreme slip bands can be observed in the deformed UFG micropillars as shown in Figure 13c,d. In addition, the observed surface morphologies provide a very clear demonstration of the occurrence of intensive GBS in the plastic deformation of the UFG materials. In the case of these UFG samples, the compensating effect of the grain boundaries has certainly converted the global maximum shear stress along a direction of 45° into the motion of individual ultrafine-grains, leading to deformation which exhibits cylindrical symmetry as rings of refined grains displaced around the sample. The observations presented in Figure 13c,d are unambiguously consistent with the smoothly stable compression load-depth curves of the UFG samples shown in Figure 12. The stable deformation by GBS of the UFG micropillars—without the occurrence of any catastrophic avalanches—emphasizes again the advantage of the sliding mechanism and suggests an important potential for using the UFG materials in the fabrication of microdevices.

5. Summary

Characterization of microstructures and mechanical properties of HPT-processed UFG Al–Zn alloys by using TEM, SEM, EDS, tensile and microhardness tests, depth-sensing indentation (DSI), micropillar compression, and DSC is reviewed. The following are the main points of the review: 1) For low Zn contents, normal strengthening was dominant, whereas for the highest Zn concentration an abnormal softening was observed due to microstructural decomposition. 2) The strong microstructure decomposition in high Zn-concentrated alloy leads also to the formation of Zn-rich grain boundary layers, which wet the Al/Al grain boundaries and enhance the role of GBS in plasticity with an unusually high SRS. 3) The present results demonstrate the importance of an enhancement in diffusion along the grain boundaries, which promotes flow by GBS. The occurrence of intensive GBS at RT in the UFG Al–30Zn alloy led to super-ductility at RT. 4) Due to the significant role of grain boundaries in plasticity of UFG materials, the deformation process is relatively homogenous and stable at the microscale without the detrimental strain avalanches. Engineering of the microstructure, for example by Zn segregations along the boundaries of aluminum grains, makes it possible to achieve superplasticity at low temperatures, and this effect may have important practical implications in electronic industry and especially for using these materials in microdevices.

Acknowledgements

This research was financed by the Hungarian-Russian bilateral Research program (TÉT) No. 2017-2.3.4-TÉT-RU-2017-00005 (N.Q.C., Sz.P., J.G.) and by the Ministry of Education and Science of the Russian Federation under grant agreement No. 14.586.21.0061 (unique project identifier RFMEFI58618X0061) (E.V.B., M.Y.M., R.Z.V.). This work was supported also by the Ministry of Human Capacities of Hungary within the ELTE University Excellence program (1783-3/2018/FEKUTSRAT).

Conflict of Interest

The authors declare no conflict of interest.

Keywords

Al–Zn alloys, grain boundary sliding, high-pressure torsion, phase decomposition, ultrafine grains

Received: June 1, 2019

Revised: July 17, 2019

Published online:

- [1] H. Löffler, *Structure and Structure Development of Al-Zn Alloys*, Akademie Verlag, Berlin, Germany **1995**.
- [2] G. A. López, E. J. Mittemeijer, B. B. Straumal, *Acta Mater.* **2004**, *52*, 4537.
- [3] B. B. Straumal, B. Baretzky, A. A. Mazilkin, F. Phillipp, O. A. Kogtenkova, M. N. Volkov, R. Z. Valiev, *Acta Mater.* **2004**, *52*, 4469.
- [4] M. Kawasaki, R. B. Figueiredo, T. G. Langdon, *Acta Mater.* **2011**, *59*, 308.
- [5] T. G. Langdon, *J. Mater. Sci.* **2009**, *44*, 5998.
- [6] M. Kawasaki, B. Ahn, T. G. Langdon, *Acta Mater.* **2010**, *58*, 919.

- [7] M. Kawasaki, T. G. Langdon, *J. Mater. Sci.* **2013**, *48*, 4730.
- [8] R. Z. Valiev, M. Y. Murashkin, A. Kilmametov, B. B. Straumal, N. Q. Chinh, T. G. Langdon, *J. Mater. Sci.* **2010**, *45*, 4718.
- [9] B. B. Straumal, R. Z. Valiev, O. A. Kogtenkova, P. Zieba, T. Czeppe, E. Bielanska, M. Faryna, *Acta Mater.* **2008**, *56*, 6123.
- [10] N. Q. Chinh, T. Györi, R. Z. Valiev, P. Szommer, G. Varga, K. Havancsák, T. G. Langdon, *MRS Commun.* **2012**, *2*, 75.
- [11] N. Q. Chinh, T. Csanádi, T. Györi, R. Z. Valiev, B. B. Straumal, M. Kawasaki, T. G. Langdon, *Mater. Sci. Eng. A* **2012**, *543*, 117.
- [12] N. Q. Chinh, R. Z. Valiev, X. Sauvage, G. Varga, K. Havancsák, M. Kawasaki, B. B. Straumal, T. G. Langdon, *Adv. Eng. Mater.* **2014**, *16*, 1000.
- [13] E. V. Bobruk, X. Sauvage, N. A. Enikeev, B. B. Straumal, R. Z. Valiev, *Rev. Adv. Mater. Sci.* **2015**, *43*, 45.
- [14] X. Sauvage, M. Yu. Murashkin, B. B. Straumal, E. V. Bobruk, R. Z. Valiev, *Adv. Eng. Mater.* **2015**, *17*, 1821.
- [15] A. Alhamidi, K. Edalati, Z. Horita, S. Hirotsawa, K. Matsuda, D. Terada, *Mater. Sci. Eng. A* **2014**, *610*, 17.
- [16] A. A. Mazilkin, B. B. Straumal, M. V. Borodachenkova, R. Z. Valiev, O. A. Kogtenkova, B. Baretzky, *Mater. Lett.* **2012**, *84*, 63.
- [17] M. V. Borodachenkova, F. Barlat, W. Wen, A. Bastos, J. J. Gracio, *Int. J. Plast.* **2015**, *68*, 150.
- [18] N. Q. Chinh, P. Jenei, J. Gubicza, E. V. Bobruk, R. Z. Valiev, *Mater. Lett.* **2017**, *186*, 334.
- [19] N. Q. Chinh, T. Csanádi, J. Gubicza, R. Z. Valiev, B. B. Straumal, T. G. Langdon, *Mater. Sci. Forum* **2010**, *667–669*, 677.
- [20] B. B. Straumal, X. Sauvage, B. Baretzky, A. A. Mazilkin, R. Z. Valiev, *Scr. Mater.* **2014**, *70*, 59.
- [21] E. O. Hall, *Proc. Phys. Soc. B* **1951**, *64*, 747.
- [22] N. J. Petch, *J. Iron Steel Inst.* **1953**, *174*, 25.
- [23] J. W. Edington, K. N. Melton, C. P. Cutler, *Prog. Mater. Sci.* **1976**, *21*, 61.
- [24] T. G. Langdon, *Acta Metall. Mater.* **1994**, *42*, 2437.
- [25] T. G. Nieh, J. Wadsworth, O. D. Sherby, *Superplasticity in Metals, Ceramics*, Cambridge University Press, Cambridge, UK **1997**
- [26] T. G. Langdon, *Acta Mater.* **2013**, *61*, 7035.
- [27] R. Z. Valiev, O. A. Kaibyshev, R. I. Kuznetsov, R. S. Musalimov, N. K. Tsenev, *Sov. Phys. Dokl.* **1988**, *33*, 626
- [28] R. Z. Valiev, Y. Estrin, Z. Horita, T.G. Langdon, M. Zehetbauer, Y. T. Zhu, *JOM* **2006**, *58*, 33.
- [29] Y. Iwahashi, Z. Horita, M. Nemoto, T. G. Langdon, *Acta Mater.* **1997**, *45*, 4733.
- [30] R. Z. Valiev, *Nat. Mater.* **2004**, *3*, 511.
- [31] R. Z. Valiev, R. K. Islamgaliev, I. V. Alexandrov, *Prog. Mater. Sci.* **2000**, *45*, 103.
- [32] A. P. Zhilyaev, T. G. Langdon, *Prog. Mater. Sci.* **2008**, *53*, 893.
- [33] A. P. Zhilyaev, G. V. Nurislamova, B. K. Kim, M. D. Baro, J. A. Szpunar, T. G. Langdon, *Acta Mater.* **2003**, *51*, 753.
- [34] G. Sakai, Z. Horita, T. G. Langdon, *Mater. Sci. Eng. A* **2005**, *393*, 344.
- [35] R. Pippan, S. Scheriau, A. Taylor, M. Hafok, A. Hohenwarter, A. Bachmaier, *Annu. Rev. Mater. Res.* **2010**, *40*, 319.
- [36] J. Zhang, N. Gao, M. J. Starink, *Mater. Sci. Eng. A* **2010**, *527*, 3472.
- [37] F. A. Mohamed, S. S. Dheda, *Mater. Sci. Eng. A* **2012**, *558*, 59.
- [38] M. J. Starink, X. Cheng, S. Yang, *Acta Mater.* **2013**, *61*, 183.
- [39] K. Edalati, Z. Horita, *Acta Mater.* **2011**, *59*, 6831.
- [40] R. Z. Valiev, T. G. Langdon, *Prog. Mater. Sci.* **2006**, *51*, 881.
- [41] T. G. Langdon, *Mater. Sci. Eng. A* **2007**, *462*, 3.
- [42] V. M. Segal, V. I. Reznikov, A. E. Drobyshevskiy, V. I. Kopylov, *Russ. Metall.* **1981**, *1*, 99.
- [43] M. Furukawa, Y. Ma, Z. Horita, M. Nemoto, R. Z. Valiev, T. G. Langdon, *Mater. Sci. Eng. A* **1998**, *241*, 122.
- [44] M. Furukawa, Z. Horita, M. Nemoto, T. G. Langdon, *J. Mater. Sci.* **2001**, *36*, 2835.
- [45] S.C. Baik, Y. Estrin, H. S. Kim, R. J. Hellmig, *Mater. Sci. Eng. A* **2003**, *351*, 86.
- [46] G. Purcek, B. S. Altan, I. Miskioglu, P. H. Ooi, *J. Mater. Proc. Technol.* **2004**, *148*, 279.
- [47] M. Kawasaki, T. G. Langdon, *Mater. Trans.* **2008**, *49*, 84.
- [48] Y. Saito, H. Utsunomiya, N. Tsuji, T. Sakai, *Acta Mater.* **1999**, *47*, 579.
- [49] M. Y. Zhan, Y. Y. Li, W. P. Chen, W. D. Chen, *J. Mater. Sci.* **2007**, *42*, 9256.
- [50] N. Q. Chinh, J. Gubicza, T. G. Langdon, *J. Mater. Sci.* **2007**, *42*, 1594.
- [51] B. B. Straumal, A. R. Kilmametov, Y. Ivanisenko, L. Kurmanaeva, B. Baretzky, Y. O. Kucheev, P. Zieba, A. Korneva, D. A. Molodov, *Mater. Lett.* **2014**, *118*, 111.
- [52] L. F. Mondolfo, *Aluminum Alloys: Structure and Properties*, Butterworths, London **1976**.
- [53] D. A. Woodford, *Trans. ASM* **1969**, *62*, 291.
- [54] Y. Song, S. Lian, *Mater. Sci. Tech.* **1989**, *5*, 443.
- [55] T. Hatayama, T. Okabe, H. Takei, *Trans. Japan Inst. Metals* **1986**, *27*, 576.
- [56] H. E. Adabbo, G. González-Doncel, O. A. Ruano, *J. Mater. Res.* **1989**, *4*, 587.
- [57] Y. M. Wang, E. Ma, *Acta Mater.* **2004**, *52*, 1699.
- [58] F. Kabirian, A. S. Khan, A. Pandey, *Int. J. Plast.* **2014**, *55*, 232.
- [59] E. Alabort, D. Putman, R. C. Reed, *Acta Mater.* **2015**, *95*, 428.
- [60] N. Q. Chinh, J. Illy, A. Juhász, J. Lendvai, *Phys. State Solid (a)* **1995**, *149*, 583.
- [61] N. Q. Chinh, P. Tasnádi, A. Juhász, I. Kovács, *J. Mater. Sci.* **1994**, *29*, 2341.
- [62] J.C. M. Li, *Mater. Sci. Eng. A* **2002**, *322*, 23.
- [63] I.-C. Choi, Y.-J. Kim, B. Ahn, M. Kawasaki, T. G. Langdon, J.-I. Jang, *Scr. Mater.* **2014**, *75*, 102.
- [64] Z. H. Cao, L. Wang, K. Hu, Y. L. Huang, X. K. Meng, *Acta Mater.* **2012**, *60*, 6742.
- [65] N. Q. Chinh, P. Szommer, *Mater. Sci. Eng. A* **2014**, *611*, 333.
- [66] M. Kawasaki, J.-I. Jang, *Materials* **2017**, *10*, 596.
- [67] V. Maier-Kiener, K. Durst, *JOM* **2017**, *69*, 2246.
- [68] N.Q. Chinh, T. Csanádi, J. Gubicza, R. Z. Valiev, *MRS Commun.* **2019**, *9*, 310.
- [69] M. A. Meyer, A. Mishra, D. J. Benson, *JOM* **2006**, *58*, 41.
- [70] H. J. Frost, M. F. Ashby: *Deformation-Mechanism Maps: The Plasticity and Creep of Metals and Ceramics*, Pergamon Press, Oxford, UK **1982**.
- [71] H. Mehrer (ed.), *Diffusion in Solid Metals and Alloys*, Landolt-Börnstein, Vol. 26, Springer, Berlin **1990**.
- [72] I. Kaur, W. Gust, L. Kosma, *Handbook of Interphase and Grain Boundary Diffusion*, Ziegler Press, Stuttgart **1989**.
- [73] K. Edalati, Z. Horita, R.Z. Valiev, *Sci. Rep.* **2018**, *8*, 6740
- [74] D. M. Dimiduk, C. Woodward, R. LeSar, M. D. Uchic, *Science* **2006**, *312*, 1188.
- [75] F. F. Csikor, C. Motz, D. Weygand, M. Zaiser, S. Zapperi, *Science* **2007**, *318*, 251.
- [76] M. D. Uchic, P. A. Shade, D. M. Dimiduk, *Ann. Rev. Mater. Res.* **2009**, *39*, 361.
- [77] P. D. Ispánovity, I. Groma, G. Györgyi, F. F. Csikor, D. Weygand, *Phys. Rev. Lett.* **2010**, *105*, 085503.
- [78] J. R. Greer, J. T. M. De Hosson, *Prog. Mater. Sci.* **2011**, *56*, 654.
- [79] P. D. Ispánovity, Á. Hegyi, I. Groma, G. Györgyi, K. Ratter, D. Weygand, *Acta Mater.* **2013**, *61*, 6234.
- [80] N. Q. Chinh, P. Szommer, Z. Horita, T. G. Langdon, *Adv. Mater.* **2006**, *18*, 34.
- [81] N.Q. Chinh, P. Szommer, T. Csanádi, T.G. Langdon, *Mater. Sci. Eng. A* **2006**, *434*, 326.
- [82] T.G. Langdon, *Mater. Sci. Eng. A* **1994**, *174*, 225.
- [83] T.G. Langdon, *J. Mater. Sci.* **2006**, *41*, 597.
- [84] T. G. Langdon, *J. Mater. Sci.* **2007**, *42*, 1782.